Research Article | Vol. 27, No. 15 / 22 July 2019 / Optics Express 20516
Optics EXPRESS

Plasmon-enhanced Ge-based metal-semiconductor-metal photodetector at near-IR wavelengths

MARIO LODARI,[1,2,4] PAOLO BIAGIONI,[1,2] MICHELE ORTOLANI,[3] LEONETTA BALDASSARRE,[3] GIOVANNI ISELLA,[1,2] AND MONICA BOLLANI[1,*]

[1] *Istitute for Photonics and Nanotechnologies, CNR, p.zza Leonardo da Vinci 32, 20133 Milano, Italy*
[2] *Dipartimento di Fisica, Politecnico di Milano, p.zza Leoardo da Vinci 32, 20133 Milano, Italy*
[3] *Dipartimento di Fisica, Sapienza Università di Roma, P.le A. Moro 2, 00185 Roma, Italy*
[4] *Current address: QuTech and Kavli Institute of Nanoscience, Delft University of Technology, 2600 GA Delft, The Netherlands*
[*] *monica.bollani@ifn.cnr.it*

Abstract: We demonstrate the use of plasmonic effects to boost the near-infrared sensitivity of metal-semiconductor-metal detectors. Plasmon-enhanced photodetection is achieved by properly optimizing Au interdigitated electrodes, micro-fabricated on Ge, a semiconductor that features a strong near IR absorption. Finite-difference time-domain simulations, photocurrent experiments and Fourier-transform IR spectroscopy are performed to validate how a relatively simple tuning of the contact geometry allows for an enhancement of the response of the device adapting it to the specific detection needs. A 2-fold gain factor in the Ge absorption characteristics is experimentally demonstrated at 1.4 μm, highlighting the potential of this approach for optoelectronic and sensing applications.

1. Introduction

Silicon-based metal-semiconductor-metal (MSM) photodetectors have become important assets in modern optoelectronics and can be applied in a wide wavelength range. However, the longer carrier lifetime and lower carrier mobility, as compared to their III-V counter parts, reduce their response speed [1]. Moreover, larger absorption volumes are needed for Si-based detectors [2,3]. An alternative is offered by germanium, which provides higher electron and hole mobilities than silicon, in addition to its full compatibility with Si-CMOS processes. Furthermore, Ge is a material of interest for light emission applications because its direct gap is only 0.140 eV above the fundamental indirect gap at 0.66 eV [4–6]. However, compared to many direct gap III-V semiconductors, Ge offers poor light emission efficiency because although the electrons are promoted to the local conduction band minimum at the Γ point, they quickly scatter into the L minimum and the non-radiative transitions are the dominant recombination mechanisms at room temperature [7]. Nevertheless, Ge MSM detectors have been actively investigated for their relatively easy fabrication and high speed performance [8,9]. Due to their lateral geometry, MSM photodetectors have a much smaller capacitance per unit area in comparison to standard p-i-n photodiodes with the same active area [10]. However, the high dark currents due to the small Schottky barrier height can limit the performance of Ge MSM photodetectors [11]. Efforts have been made to improve the optical response by coupling the photodetector to a waveguide [12], or by modulating the Schottky barrier height in order to reduce the dark currents using amorphous Ge, GeO_x and SiC thin layers [13–15]. The response time could also be reduced down to a few tens of picoseconds by pushing the spacing between the electrode fingers close to the optical diffraction limit [16,17]. However, this downsizing of the electrode spacing decreases

#365588 https://doi.org/10.1364/OE.27.020516
Journal © 2019 Received 26 Apr 2019; revised 5 Jun 2019; accepted 10 Jun 2019; published 9 Jul 2019

Optics EXPRESS

the active area, thus resulting in photodetector sensitivity degradation. Thanks to a suitable periodic ordering of the metallic contacts, surface plasmon polaritons (SPPs) can be exploited to overcome this limitation. Metallic gratings have also been used to promote and boost the hot electron detection mechanism, together with the free carrier absorption mechanism [18,19]. Here we propose to exploit a plasmonic grating to be applied to the MSM geometry in order to exploit in-plane diffraction as an enhancement mechanism. This photodetector can in fact be turned into a plasmonic grating, tailoring the absorption spectrum of the underlying material for specific applications, concentrating light and enhancing the absorption at specific wavelengths of the active material. The interaction, indeed, between confined light and matter gives rise to a plethora of effects that can be exploited as transduction systems to gain the sensitivity and resolution needed also in a vast number of other applications, from biology to aerospace. In this work, we design, fabricate, and experimentally characterize a plasmon-enhanced Ge based MSM photodetector showing how a relatively simple adjusting of the periodicity and lateral dimensions of the metallic geometry allows for a straightforward enhancement of the response of the device. A full characterization of the device performance is out of the scope of this paper, therefore parameters such as detectivity, noise equivalent power, photoresponse speed and so on are not discussed here. Moreover, there is plenty of room for improvements to push the device response, such as exploiting a specific Ge thickness to introduce cavity enhancement or adopting different filling factors to optimize the electrode distance. However, the aim of this work is not focused on presenting an optimized photodetector, but to show how the photodetector responsivity can be significantly improved by simply adjusting the periodicity of the grating contacts.

2. The experiment

As active material, a 1 μm thick slightly n-doped Ge ($n = 4 \times 10^{15}$ cm^{-3}) film is grown on Si substrates by low-energy plasma-enhanced chemical vapor deposition, using a high rate deposition of about 4 nm/s at 500 °C [20]. An in-situ annealing procedure over six cycles between 600 and 800 °C is performed in order to reduce the threading dislocations density below $7 \pm 0.5 \times 10^7$ cm^{-2}. Preferential etching techniques are used to estimate the threading dislocation density in the Ge substrate, using a solution of 10 mL HF (50% vol) + 15 mL HNO_3 (69% vol) + 1 mg KI + 1 mg I_2 + 5 mL CH_3COOH (100%vol) + 60 mL H_2O at a temperature of 273 K for 30 s [21] and the counting statistics is performed on etched surfaces imaged by atomic force microscopy. A two-layer positive tone resist is spin coated on cleaned Ge surface, exposed and developed accordingly to a standard e-beam lithography procedure. Finally, 100 nm thick pure gold is deposited by e-beam evaporation: the gold is used to concurrently exploit its plasmonic properties and provide Schottky contact with the Ge.

In the optical setup, the light emitted by a halogen lamp is monochromatized, focused by a system of lenses, and chopped at 391 Hz. A 650 nm visible light is used during the alignment operations, and a two-probe I-V setup is used to bias the device under measurement by 0.5 V. This value of the bias has been selected because, although remaining reasonably low and thus ensuring linearity, it provides a good signal-to-noise ratio. In order to compare the spectral response of the device responsivity, the light source is first characterized with a commercial photodetector, considering two orthogonal linear polarizations because of the polarization-dependence behavior in the plasmonic grating. One linear polarization is oriented parallel to the fingers main axis, while the other one is orthogonal to it as sketched in Fig. 1. A standard lock-in technique is used to isolate the photocurrent signal, and a transimpedance amplifier is used to convert the current to voltage and amplify it by a factor of 10^5 V/A. Concerning the Fourier-transform spectroscopic measurements, a specular reflection geometry with a cassegrain objective (15x, Bruker Hyperion) is used.

Optics EXPRESS

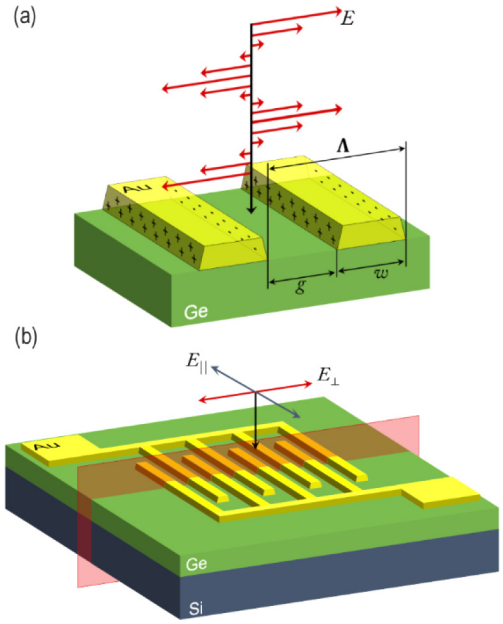

Fig. 1. (a) Cartoon of a metallic grating. Λ, w and g are the grating periodicity, the width and the spacing of the metallic fingers. Normal illumination and an electric field polarization orthogonal to the metal grating elements are taken into account. The accumulated charges on the structure front ends are also illustrated. The metallic fingers length and thickness are fixed to 250 μm and t = 100 nm, respectively (b) Sketch of the simulated final device showing parallel $E_{\parallel}$ and orthogonal $E_{\perp}$ electric field polarization components. The simulated device cross section is outlined in red.

3. Results and discussion

The MSM metallic fingers are used to couple the light with the collective electron oscillations in the contact structure at a specific incident wavelength $\bar{\lambda}$. Thanks to the momentum $k_g = \frac{2\pi}{\Lambda}$ provided by a grating of periodicity Λ, and their peculiar planar geometry, the MSM interdigitated photodetectors are eligible to improve their performance due to a resonant plasmonic enhancement boosted by the grating diffraction [18,22–24]. To be effective, the incident electric field must be orthogonal to the longitudinal direction of the interdigitated fingers, and the grating periodicity has to be suitably designed to achieve plasmonic enhancement at a given $\bar{\lambda}$. A cartoon is reported in Fig. 1(a), where Λ, w, g and E correspond to the period of the grating, the metal finger width, the gap between them and the electric field amplitude, respectively. A sketch of the final device is reported in Fig. 1(b), where $E_{\parallel}$ and $E_{\perp}$ are the parallel and orthogonal electric field polarization components considered for the experimental characterization of the devices.

To demonstrate how the plasmonic grating affects the photodetector performance, three types of devices (called A, B and C) with different metallic grating periodicities Λ are considered. The metallic fingers length and thickness are fixed to $l = 250$ µm and $t = 100$ nm, respectively (Fig. 2). In particular, device C is designed to be resonant at a wavelength about $\bar{\lambda} = 1.4$ µm by relying on numerical simulations, as discussed below.

The number of finger pairs n is adapted according to their width w and spacing g, in order to design and fabricate all the devices with the same active area using a filling factor of 0.5 ($g = w$). In the devices A and B the widths of the fingers are adapted in order to represent a non-resonant reference, by using spacings and widths much larger than the wavelength of interest. The device C, on the other side, is designed according to the design described previously.

Optics EXPRESS

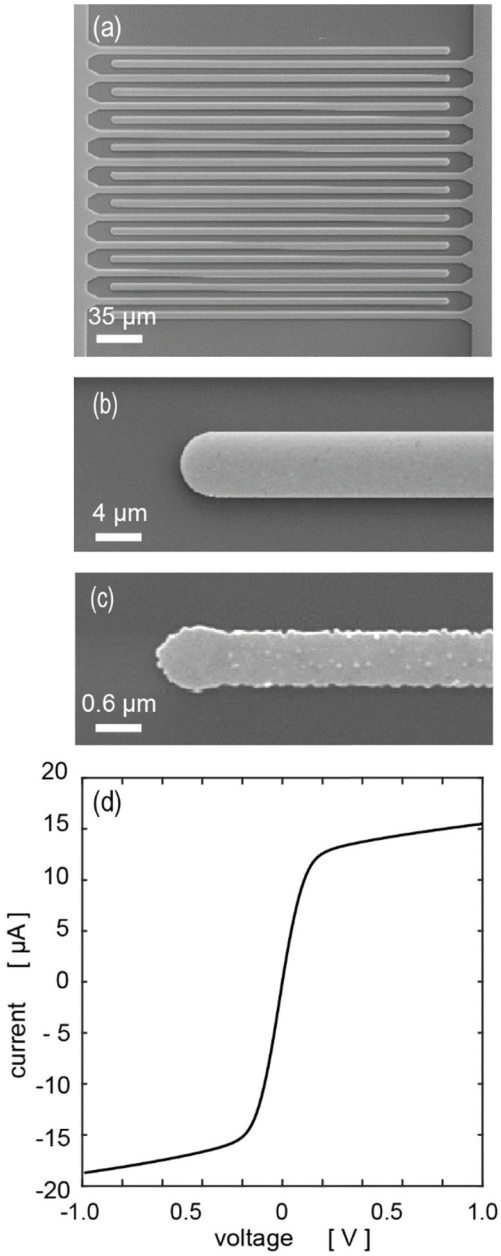

Fig. 2. Plan view SEM micrographs of (a) the interdigitated fingers of the B device, and (b,c) details of the B and C devices fingers. (d) Characteristic I-V curve from a fabricated interdigitated Ge Schottky MSM device. The geometrical parameters of the A, B and C devices are the following: $w_A(=g_A) = 10\,\mu m$, n_A=5, and $\Lambda_A = 20\,\mu m$; $w_B(=g_B) = 5\,\mu m$, n_B=10, and Λ_B=10 µm; $w_C(=g_C) = 0.65\,\mu m$, n_C=85, and Λ_C=1.30 µm.

Optics EXPRESS

A representative DC electrical characterization of one of the investigated devices, reported in Fig. 2(d), demonstrates a typical I-V curve from a Schottky MSM detector. The Schottky barrier heights of the Ge-Au contacts, extracted from a fitting procedure [25], show values of about 0.59 eV.

Simulations are performed to investigate how Λ affects the performance of the devices. Due to the MSM geometry, the system cross-section is considered in the two-dimensional simulations, according to the sketch in Fig. 1(b). The simulated system consists in a 1 μm-thick Ge film on a Si bulk substrate, on top of which the Au MSM fingers are located, considering different widths w and spacing g. In order to verify the effectiveness of the approach, FDTD simulations are performed to calculate the electric field distribution and the optical absorption in the designed devices [26]. To mimic the actual experimental configuration, we simulate an extended device illuminated by a focused Gaussian beam with a beam waist of about 15 μm. In order to avoid reflection contributions from the outer regions, perfectly matched layer (PML) boundary conditions are applied. Anti-symmetric boundary conditions are used instead at the center of the simulated area in order to exploit the system symmetry and reduce the computational time. In Fig. 3, the resulting absorbed power densities from the simulated devices are demonstrated, reporting the enhancement by the resonance at around 1.4 μm in the device C. All maps are captured around the center of the device, i.e. at the central position of the illumination Gaussian beam. The electric field polarization is orthogonally oriented to the metallic finger main axis, as shown by $E_\perp$ in Fig. 1. The permittivities are modeled with experimental values from the literature by using built-in fitting functions [27,28].

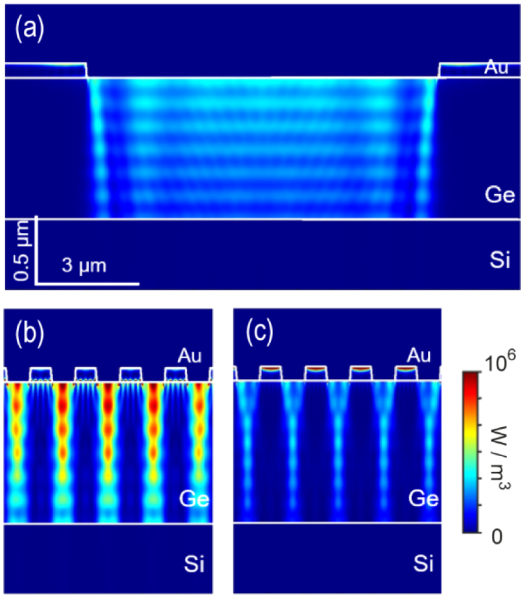

Fig. 3. The simulated absorption distribution (50×10 μm^2 two-dimensional simulation area) of (a) the non-resonant device B and (b) the resonant device C, considering a 1.4 μm illuminating wavelength. (c) The absorption distribution of resonant device C simulated at a non-resonant wavelength of 1.2 μm. Non uniform scales are used along the directions orthogonal and parallel to the interface.

The two absorption maps in panels (a) and (b) of Fig. 3 show the difference between the non-resonant B and the resonant C devices respectively, considering an illuminating $\lambda = 1.4$ μm and an incident power density of 1 W/m^2. While in the device B the metallic contacts do not introduce any particular effect, in the C configuration a strong field enhancement is provided. In

Optics EXPRESS

fact, both the field intensity and the consequent absorption are strongly improved, leading to a higher expected absorption characteristics at the considered λ. In order to remark the resonance effect, the non-resonant absorption at $\lambda = 1.2\,\mu m$ of device C is also shown in Fig. 3(c), where the absorption values are significantly lower than those registered at 1.4 µm and comparable to those reported for the device B.

The spectral response of the considered devices is also calculated from the performed simulations via standard Fourier transformation as customary in FDTD methods. The simulated absorption spectra for the three devices are shown in Fig. 4(a). Comparing the three absorption curves, a significant modification can be observed. A resonance peak emerges around 1.4 µm for the device C for linear polarization perpendicular to the grating, which provides a boosting factor of about 2 with respect to the non-resonant values of devices A and B. The additional oscillating features in the 1.0-1.5 µm wavelength range, which are visible in all devices, are attributed to Fabry-Perot etaloning in the Ge film (visible also in the absorption distribution profile in Fig. 3). While the absorption maps in Fig. 3 demonstrate the distribution of the absorbed power density for the whole device (also inside the Au contacts), the calculations in Fig. 4(a) plot the integral of such a power density over the semiconductor volume. Photocurrent experiments are then carried out in order to confirm the simulation findings. The results are reported in Figs. 4(b) and (c), where a Savitzky-Golay digital filter is applied in order to reduce the noise that affects the measurements [29].

In order to rule out any artifact due to the non-homogeneous lamp emission spectrum in the considered range, the responsivity $R(\lambda) = I_{pc}(\lambda)/P_0(\lambda)$ is used to compare the devices, where I_{pc} and P_o are the detected photocurrent signal and the incident optical power. Considering the devices A and B, the polarization induces no noticeable differences in the values of $R\ (\lambda)$ reported in Figs. 4(b) and (c). On the other hand, in the resonantly designed C case, a strong difference in magnitude and shape can be observed between the $R_\perp$ and $R_\parallel$ components. A resonance peak is clearly observed around 1.4 µm in the orthogonal configuration, which is instead not visible in the parallel one. The effectiveness of the approach is therefore confirmed experimentally, and a roughly 2-fold enhancement is reported and confirmed at the resonant λ as anticipated by the simulations.

The reported responsivity values represent a lower boundary of the actual values. In fact, because of the exploited experimental setup, the illuminating spot size is larger than the active area of the devices, leading to an overestimation of the illuminating power and a consequent underestimation of R. Only lower boundary estimations can be given also concerning the external quantum efficiency (EQE), given by $EQE = \frac{hcR}{e\lambda}$, where h is the Planck's constant, c is the velocity of light and e the electron charge. Considering the resonant device C, at a wavelength of 1.4 µm, values of 0.23 and 0.12 are found with a perpendicular and parallel polarization respectively.

In order to independently confirm the simulation and experimental results, Fourier- Transform IR (FTIR) spectroscopy is also carried out and reported in Fig. 5.

While the absorption resonance results in a maximum in the photocurrent spectrum, the reflected light is expected to feature a dip at the same resonant λ because absorbed radiation is not reflected at specular angle. The spectra in Fig. 5 indeed demonstrate a dip in the experimental reflectivity of the device C, here located around 1.7-1.8 µm, which is consistent with the shift of the 1.4 µm resonance of sample C to longer wavelengths due to the non-normal reflection geometry (incidence angle θ spanning roughly between 15° and 30°, as determined by the cassegrain illumination). The dip in the specular-angle reflectivity shifting with the incidence angle is related to the collective response that is established thanks to the in-phase excitation of each individual grating element, i.e. to the establishment of a diffraction order propagating along the plane of the grating, according to the relation:

$$\bar{k}_\parallel + \frac{2\pi}{\Lambda} = \frac{2\pi}{\lambda}$$

Optics EXPRESS

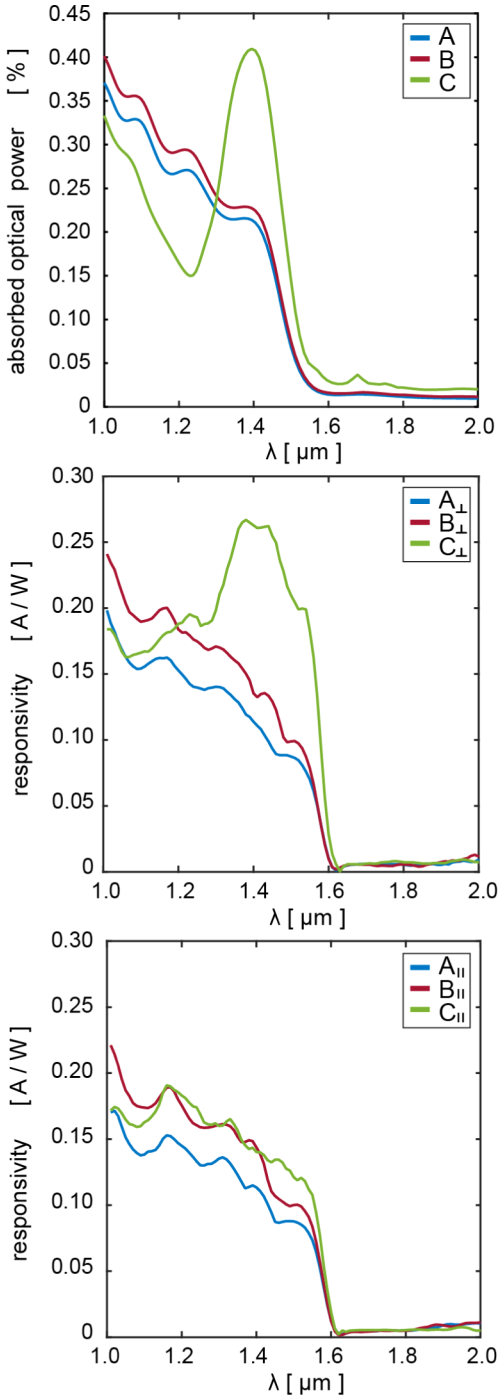

Fig. 4. (a) The absorption spectra vs. λ of the three simulated A, B and C devices are reported in blue, red and green respectively. The experimental responsivity vs. λ for (b) the orthogonal and (c) the parallel field configuration are reported. A Savitzky-Golay digital filter, with polynomial order of 3 and a frame length of 11, is used.

Optics EXPRESS

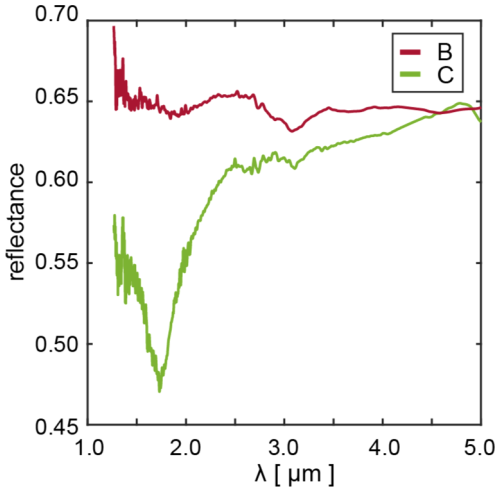

Fig. 5. The FTIR reflectance spectra vs. the wavelength λ of the non-resonant B and the resonant C devices (red and green curves, respectively).

In summary, in this work Ge MSM photodetectors are successfully turned into plasmonic gratings demonstrating how the photodetector responsivity can be significantly improved by simply adjusting the periodicity of the metallic grating. A significant 2-fold gain factor at 1.4 μm without adding any additional step to the standard fabrication procedure is obtained. Since the proposed approach is very general, it can be adapted to tune the resonant responsivity at a desired wavelength by choosing suitable active materials, plasmonic metals, and grating periodicities. Furthermore, due to the strong influence that the environment has on the dielectric/metal interface and in the SPPs generation, such devices can be also adopted in perspective sensing applications, relying on the fact that the demonstrated enhancement mechanism can be universally applied to this class of devices.

Funding

Ministero dell'Istruzione, dell'Università e della Ricerca (MIUR) (RBSI14IT0D); Regione Lombardia (7784/2016, III Accordo Quadro).

References

1. R. Liu, L. Jones, D. Liao, D. Samara-Rubio, O. Rubin, R. Cohen, M. A. Nicolaescu, and Paniccia, "A high-speed silicon optical modulator based on a metal–oxide–semiconductor capacitor," Nature **427**(6975), 615–618 (2004).
2. C. Buchal, M. Löken, T. Lipinsky, L. Kappius, and S. Mantl, "Ultrafast silicon based photodetectors," J. Vac. Sci. Technol., A **18**(2), 630–634 (2000).
3. P. Eng, S. Song, and B. Ping, "State-of-the-art photodetectors for optoelectronic integration at telecommunication wavelength," Nanophotonics **4**(3), 277 (2015).
4. M. Rouvière, L. Vivien, X. L. Roux, J. Mangeney, P. Crozat, C. Hoarau, E. Cassan, D. Pascal, S. Lavel, J.-M. Fédéli, J.-F. Damlencourt, J. M. Hartmann, and S. Kolev, "Ultrahigh speed germanium-on-silicon-on-insulator photodetectors for 1.31 and 1.55 μm Operation," Appl. Phys. Lett. **87**(23), 231109 (2005).
5. M. J. Süess, R. Geiger, R. A. Minamisawa, G. Schiefler, J. Frigerio, D. Chrastina, G. Isella, R. Spolenak, J. Faist, and H. Sigg, "Analysis of enhanced light emission from highly strained germanium micro bridges," Nat. Photonics **7**(6), 466–472 (2013).
6. V. Giliberti, E. Sakat, M. Bollani, V. Altoe, M. Melli, A. Weber-Bargioni, L. Baldassarre, M. Celebrano, J. Frigerio, G. Isella, S. Cabrini, and M. Ortolani, "Functionalization of Scanning Probe Tips with Epitaxial Semiconductor Layers," Small Methods **1**(3), 1600033 (2017).
7. C. Lange, N. S. Köster, S. Chatterjee, H. Sigg, D. Chrastina, G. Isella, H. von Känel, B. Kunert, and W. Stolz, "Comparison of ultrafast carrier thermalization in GaxIn1−xAs and Ge quantum wells," Phys. Rev. B **81**(4), 045320 (2010).

Optics EXPRESS

8. L. Cao, J. S. Park, P. Fan, B. Clemens, and M. L. Brongersma, "Resonant Germanium Nanoantenna Photodetectors," Nano Lett. **10**(4), 1229–1233 (2010).
9. J. Oh, S. Csutak, and C. Campbell, "High-speed interdigitated Ge PIN photodetectors," IEEE Photonics Technol. Lett. **14**(3), 369–371 (2002).
10. J. Michel, J. Liu, and L. C. Kimerling, "High-performance Ge-on-Si photodetectors," Nat. Photonics **4**(8), 527–534 (2010).
11. J. Wang and S. Lee, "Ge-Photodetectors for Si-Based Optoelectronic Integration," Sensors **11**(1), 696–718 (2011).
12. C. Y. Ahn, J. Hong, W. Liu, M. Giziewicz, L. Beals, J. Kimerling, J. Michel, F. Chen, and Kärtner, "High performance, waveguide integrated Ge photodetectors," Opt. Express **15**(7), 3916 (2007).
13. J. Oh, S. Banerjee, and J. Campbell, "Metal-germanium-metal photodetectors on heteroepitaxial Ge-on-Si with amorphous Ge Schottky barrier enhancement layers," IEEE Photonics Technol. Lett. **16**(2), 581–583 (2004).
14. T. Nishimura, K. Kita, and A. Toriumi, "A Significant Shift of Schottky Barrier Heights at Strongly Pinned Metal/Germanium Interface by Inserting an Ultra-Thin Insulating Film," Appl. Phys. Express **1**, 051406 (2008).
15. K. W. Ang, S. Y. Zhu, J. Wang, K. T. Chua, M. B. Yu, G. Q. Lo, and D. L. Kwong, "Novel Silicon-Carbon (Si:C) Schottky Barrier Enhancement Layer for Dark-Current Suppression in Ge-on-SOI MSM Photodetectors," IEEE Electron Device Lett. **29**(7), 704–707 (2008).
16. J. Guo, Z. Wu, Y. Li, and Y. Zhao, "Design of plasmonic photodetector with high absorptance and nano-scale active regions," Opt. Express **24**(16), 18229 (2016).
17. L. Augel, Y. Kawaguchi, S. Bechler, R. Karner, J. Schulze, H. Uchida, and I. A. Fischer, "Integrated Collinear Refractive Index Sensor with Ge PIN Photodiodes," ACS Photonics **5**(11), 4586–4593 (2018).
18. G. Tagliabue, A. S. Jermyn, R. Sundararaman, A. J. Welch, J. S. DuChene, R. Pala, A. R. Davoyan, P. Narang, and H. A. Atwater, "Quantifying the role of surface plasmon excitationand hot carrier transport in plasmonic devices," Nat. Commun. **9**(1), 3394 (2018).
19. H. Chalabi, D. Schoen, and M. L. Brongersma, "Hot-Electron Photodetection with a Plasmonic Nanostripe Antenna," Nano Lett. **14**(3), 1374–1380 (2014).
20. D. Chrastina, G. Isella, B. Rössner, M. Bollani, E. Müller, T. Hackbarth, and H. Von Känel, "High quality SiGe electronic material grown by low energy plasma enhanced chemical vapour deposition," Thin Solid Films **459**(1-2), 37–40 (2004).
21. A. Sammak, D. Sabbagh, N. W. Hendrickx, M. Lodari, B. Paquelet Wuetz, A. Tosato, L. Yeoh, M. Bollani, M. Virgilio, M. Andreas Schubert, P. Zaumseil, G. Capellini, M. Veldhorst, and G. Scappucci, "Shallow and Undoped Germanium Quantum Wells: A Playground for Spin and Hybrid Quantum Technology," Adv. Funct. Mater. **29**(14), 1807613 (2019).
22. Q. Cao and P. Lalanne, "Negative Role of Surface Plasmons in the Transmission of Metallic Gratings with Very Narrow Slits," Phys. Rev. Lett. **88**(5), 057403 (2002).
23. Z. Yu, G. Veronis, S. Fan, and M. L. Brongersma, "Design of Mid Infrared Photodetectors Enhanced by Surface Plasmons on Grating Structures," Appl. Phys. Lett. **89**(15), 151116 (2006).
24. R. D. R. Bhat, N. C. Panoiu, S. R. J. Brueck, and R. M. Osgood, "Enhancing the signal to-noise ratio of an infrared photodetector with a circular metal grating," Opt. Express **16**(7), 4588 (2008).
25. R. Nouchi, "Extraction of the Schottky parameters in metal - semiconductor – metal diodes from a single current - voltage measurement," J. Appl. Phys. **116**(18), 184505 (2014).
26. FDTD Solutions, Lumerical Solutions, Inc., Canada
27. P. B. Johnson and R. W. Christy, "Optical Constants of the Noble Metals," Phys. Rev. B **6**(12), 4370–4379 (1972).
28. Palik, ed. Handbook of Optical Constants of Solids (Academic Press, Orlando, 1985)
29. A. Savitzky and M. J. E. Golay, "Smoothing and Differentiation of Data by Simplified Least Squares Procedures," Anal. Chem. **36**(8), 1627–1639 (1964).